

International Journal of Crashworthiness



ISSN: 1358-8265 (Print) 1754-2111 (Online) Journal homepage: www.tandfonline.com/journals/tcrs20

Crashworthiness evaluation of urban air mobility vehicle configurations using a simplified finite element modelling approach

Paul Schatrow, Matthias Waimer & Marius Lützenburger

To cite this article: Paul Schatrow, Matthias Waimer & Marius Lützenburger (19 Nov 2025): Crashworthiness evaluation of urban air mobility vehicle configurations using a simplified finite element modelling approach, International Journal of Crashworthiness, DOI: 10.1080/13588265.2025.2588900

To link to this article: https://doi.org/10.1080/13588265.2025.2588900

9	© 2025 The Author(s). Published by Informa UK Limited, trading as Taylor & Francis Group
	Published online: 19 Nov 2025.
	Submit your article to this journal 🗷
hil	Article views: 74
α	View related articles 🗷
CrossMark	View Crossmark data 🗹



∂ OPEN ACCESS \



Crashworthiness evaluation of urban air mobility vehicle configurations using a simplified finite element modelling approach

Paul Schatrow (D), Matthias Waimer and Marius Lützenburger

German Aerospace Center (DLR), Institute of Structures and Design, Stuttgart, Germany

ABSTRACT

This paper presents a crashworthiness evaluation of selected electric vertical take-off and landing (eVTOL) 'lift+cruise' configurations based on finite element simulation in an early conceptual design phase. A simplified macro-FE modelling approach is used and the performed simulations consider crash load cases with aspects from real-world accident scenarios to ensure robust crash safety in the design process. The paper discusses the developed modelling approach and presents detailed results of the finite element simulations performed for different eVTOL configurations and various crash load cases.

ARTICLE HISTORY

Received 29 November 2023 Accepted 9 November 2025

KEYWORDS

Crashworthiness; urban air mobility; eVTOL configurations; conceptual design; finite element simulation

1. Introduction

In recent times, some key technologies have been developed that enable concepts for electric vertical take-off and landing (eVTOL) aircraft which may become an alternative mode of transportation for urban and regional mobility. Key technologies such as distributed electric propulsion (DEP), autonomous flight technology and 5 G communication networks have been developed which are likely to expand urban mobility to include urban air mobility (UAM) in the next decades. Various studies on the future UAM market situation and the expected timelines for introducing eVTOLs for commercial passenger transportation have been published and highlight the probability of a factual change in the urban mobility [1–6].

In October 2020, the Vertical Flight Society listed 349 different vehicle concepts in its eVTOL Aircraft Directory [7] with a large variety of different architectures and lift and thrust concepts. From October 2020 to May 2023, this number increased from 349 to 817 different vehicle concepts listed in this directory. Besides the underlying range of different UAM missions – from intra- to inter-city missions – especially DEP is the key technology that drives this concept diversity.

From a crashworthiness point of view, this new design freedom is an opportunity and a risk at the same time. Novel aircraft architectures, including all aspects of electric flight, need to consider crashworthiness aspects already in the conceptual design phase to reduce any risk of costly and complicated design changes at a later stage and to take the opportunity to utilise the aircraft architecture for improved

crashworthiness. This is the motivation of the research work presented in this paper.

The paper first deals with crashworthiness requirements and derives crash load cases which are considered in this study, see Section 2. Hereafter, a simplified modelling approach for crashworthiness evaluation using finite element simulation in the conceptual design phase is presented in Section 3. This developed simulation method was applied to different eVTOL concepts for crashworthiness evaluation. Results of this simulation study are presented in Section 4. Final conclusions are given in Section 5.

The presented crashworthiness evaluation considers eVTOL concepts of the 'lift+cruise' category which describes vehicle architectures with completely independent thrusters used for cruise versus for lift without any thrust vectoring [7]. Lift during vertical take-off and landing is provided by thrusters whereas for the cruise mode wing lift is used. Hence, this vehicle category's characteristics are a fixed wing, several thrust units, and typically also engine beams for thrust unit installations.

The top-level aircraft requirements (TLARs) for the eVTOL concepts considered in this study are: Four occupants and a range between 60 and 80 km.

2. Crashworthiness requirements and crash load cases

Certification aspects for eVTOL crashworthiness in the context of commercial UAM missions are not yet fully clarified, in particular with regard to acceptable means of compliance, although significant progress is achieved by the authorities.

Civil aviation authorities (CAAs) have worked out rules and guidance material for certification of eVTOL aircraft, with slightly different approaches. The European Union Aviation Safety Agency (EASA) has published special conditions and proposed means of compliance [8-11] whereas the Federal Aviation Administration (FAA) follows a case-to-case decision [12] and has published first special class airworthiness criteria [13,14]. Both approaches are taking into account aspects from the small aeroplane category (14 CFR Part 23/ CS 23) and small rotorcraft category (14 CFR Part 27/CS 27), and it can be expected that future means of compliance will be defined close to the existing framework which is mainly based on the emergency landing conditions (Part/CS 23/27.561), emergency landing dynamic conditions (Part/CS 23/27.562), and fuel system/energy storage crash resistance (Part/CS 27.952) [12,15] - enabling also less prescriptive certification approaches based on the latest certification specification amendments providing performance-based rules [8,16]. However, research organisations and further associations demand for alternative approaches beyond the traditional dynamic seat approach (Part/CS 23/27.562) to improve occupant safety [17-21]. Taking into account the expected enormous number of flight hours [1-6], the historic safety approach to prevent accidents is challenged as, on a probability basis, accidents are highly likely to occur and a crash safety approach along the lines of the automotive industry is being called for [18-24]. A system-level approach is proposed utilising the entire available structural space for occupant protection and considering a cascading system of, e.g. landing gear, airframe structure and seats for energy absorption. Using finite element analysis for two different eVTOL configurations it could be demonstrated that the 1,500 lb lumbar load criterion according to Part/CS 23/ 27.562 can be met for vertical impact conditions of 9.14 m/s (30 ft/s), by using a system-level approach [25,26].

In this sense, the research work presented in this paper partly focuses on crashworthiness beyond the regulatory specifications with the aim to demonstrate how crashworthiness evaluation can be performed in an early conceptual design phase leading to the potential of convincing cost versus safety benefit solutions for crashworthy eVTOL concepts.

2.1. Crash load cases

The crash load cases defined in this study were derived from representative UAM missions [27-29], considering UAM specific mission characteristics such as critical lift transition phases at low altitude or flights over different terrain. Similar to rotorcraft, comparably high off-axis crash impact conditions are expected for typical accident scenarios in an urban environment.

For this reason, the focus of this study was laid on the crash energy absorption management providing robust crash performance under real-world impact conditions including off-axis loading and combined vertical/horizontal impact conditions.

The crash load cases considered in the simulation study are presented in Table 1. Load case '#0' refers to the landing gear limit drop test (Part/CS 27.725) and was used for adjustments of the landing gear model to comply with the certification specifications.

Load cases '#1' - '#5' served for the adjustment of the vehicle's crash energy absorption management. Load case '#2' is the reference design load case which assumes a vertical impact velocity of $v_z = 8 \,\text{m/s}$. The underlaying assumption for this vertical impact speed is a critical event during the transition phase at 12-15 m altitude and sufficient residual thrust for a partially controlled descent resulting in crashworthy emergency landing conditions [12]. Using load cases '#1' - '#5', sufficient crashworthiness is demonstrated for impact conditions beyond the reference design load case, up to a vertical impact velocity of $v_z = 10 \,\text{m/s}$ (load case '#3'), and also for crash scenarios with reduced impact energy (load cases '#1', '#4', '#5').

Sufficient crash performance under real-world impact conditions is demonstrated using load cases '#6' - '#14', with off-axis loading under purely vertical impact conditions represented by load cases '#6' - '#8', and combined vertical/ horizontal impact conditions represented by load cases '#9' -'#14'. The horizontal impact velocity of $v_x = 25 \,\text{m/s}$ represents an assumption for an emergency landing with horizontal impact speed equal to 1.2 times stall speed, and v_x = 40 m/s represents a challenging robustness load case for which a reasonable crash performance has to be shown. Additionally, load cases '#11' and '#14' were defined with an

Tuble II besign	road cases dein		ididition in the	conceptual desig	p.i.ase.		
Load case [-]	v _z [m/s]	v _x [m/s]	Roll [°]	Pitch [°]	Yaw [°]	Terrain [-]	Payload [%]
#0	2.5	0	0	0	0	hard	100
#1	4	0	0	0	0	hard	100

Table 1. Design load cases defined for crash simulation in the conceptual design phase

#0	2.5	0	0	0	0	hard	100	66.6
#1	4	0	0	0	0	hard	100	0
#2	8	0	0	0	0	hard	100	0
#3	10	0	0	0	0	hard	100	0
#4	8	0	0	0	0	hard	50	0
#5	4	0	0	0	0	hard	50	0
#6	8	0	-10	0	0	hard	100	0
#7	8	0	0	10	0	hard	100	0
#8	8	0	0	-10	0	hard	100	0
#9	8	25	0	0	0	hard	100	0
#10	8	25	-10	10	-10	hard	100	0
#11	8	25	-10	10	-10	soft*	100	0
#12	8	40	0	0	0	hard	100	0
#13	8	40	-10	10	-10	hard	100	0
#14	8	40	-10	10	-10	soft*	100	0

^{*}Soft terrain: Simplified simulation of soft soil ploughing using an increased friction coefficient, still with hard surface.

increased friction coefficient $\mu = 0.8$ to simulate soft soil ploughing and to induce higher longitudinal loads in the vehicle structure.

3. Model description

This section provides an overview of the selected modelling approach and simulation model details. All simulations were performed using the explicit finite element (FE) solver LS-Dyna, some modelling options are FE code specific.

3.1. Modelling approach for crashworthiness evaluation in the conceptual design phase

An effective modelling approach for crash simulation in the conceptual design phase concentrates on the investigation of vehicle architecture and general design features to support main decisions in the design process. Structural elements that contribute to the crash kinematics and energy absorption are modelled in a simple and efficient way, partly using macro elements for describing structural failure by force-displacement or moment-rotation curve input data. Other structural details are neglected and it is presumed that these details will be developed in the later design stages according to acknowledged crash design principles [30-32]. Neglecting structural details supports a simplified modelling and results in efficient computation time, which is crucial for performing various simulation runs of different design concepts and load cases.

This so-called macro-FE modelling approach has been developed and applied in the past for preliminary design studies [33,34] and was transferred in this present study to conceptual design applications for which most structural details are not yet defined.

Based on the needs and the available data in an early conceptual design phase, the selected macro-FE modelling approach discretizes the main airframe structure by a frame work of beam elements that represent the frames, stringers, crossbeams, ribs, spars, etc. Hence, the cross-sectional definition of these structural elements can easily be defined and adapted by the beam element input data without adapting the FE mesh. In addition, the airframe skin is modelled using shell elements to incorporate the skin's shear stiffening function that may have a significant effect especially under combined vertical/horizontal impact conditions for which, e.g. airframe upper deck masses may introduce high shear loads.

Following this simplified and efficient modelling approach, different structural components such as wing, fuselage, landing gear etc. are connected to each other using the LS-Dyna constraint function *CONSTRAINED INTERPOLATION. Likewise, the same constraint function is used to connect single mass elements to the structure that represent battery packs, power units, luggage and other single mass items.

Main structural failure that contributes to the crash kinematics and main energy absorption is described using connector elements (beam formulation 6 and material type *MAT_119/*MAT_GENERAL_NONLINEAR_6DOF_ DISCRETE_BEAM) with individual force-displacement characteristics that easily can be modified to improve the vehicle crash performance and finally to determine the structural failure characteristics required to obtain crash safety. Those connector elements are installed in the subfloor structure (axial crushing), the engine beams (axial crushing) and the landing gear (oleo strut compression & crash absorber axial crushing).

The occupants on their seats are modelled using a simplified system of connector elements (beam formulation 6 and material type *MAT_121/*MAT_GENERAL_NONLINEAR_ 1DOF DISCRETE BEAM) representing the seat stroke functionality and the seat cushion characteristics as well as (beam formulation 6 and material type *MAT_146/*MAT_ 1DOF_GENERALIZED_SPRING) representing the occupant's lumbar spine according to the DRI model [35,36].

An overview on the selected macro-FE modelling approach is depicted in Figure 1. An alternative modelling approach for crash simulation in the conceptual design is the multibody simulation approach as applied in other research work

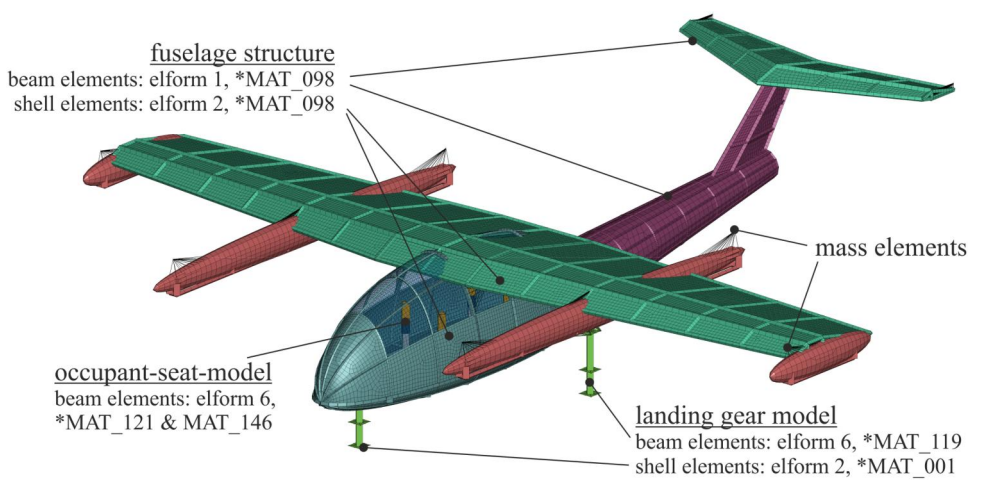


Figure 1. Selected macro-FE modelling approach.

[20,37,38]. Compared to a multibody approach, the advantage of the macro-FE modelling approach is the capability of variable Discretisation refinement towards full FE simulations within the progressing design phases.

3.2. Macro-FE modelling details

The macro elements for representation of main structural failure are shown in Figure 2 for eVTOL designs with different wing configuration as discussed later in Section 4: Highwing configuration (HWC), mid-wing configuration (MWC) and low-wing configuration (LWC). All considered macro elements represent energy absorption, respectively load limitation, under axial compression and are located in the subfloor structure, in the inner and outer engine beams, in the landing gear and in the seats. The macro element input characteristics are given in Figure 3, exemplarily for the MW-configuration. Note that other structural parts, not intended as main energy absorbing structures, can also contribute to structural failure and minor energy absorption according to the modelling details described in Section 3.4.

This contribution to energy absorption can be considered small while the major energy absorption is provided by the main crash structures modelled with macro elements.

The landing gear is modelled as a serial system of an oleo strut with shock absorption characteristics (Figure 3a) and an axial crush absorber (Figure 3b).

The landing gear oleo strut is designed to comply with CS 27.725 'Limit drop test' and CS 27.473 'Ground loading conditions and assumptions'. The assumption for the landing gear oleo strut is based on literature data [39] which describes a landing gear design for a CS-23 small aeroplane. The characteristics of the main and nose landing gear oleo struts were individually adapted for the different eVTOL configurations and depend on the position of the centre of mass relative to the landing gear position.

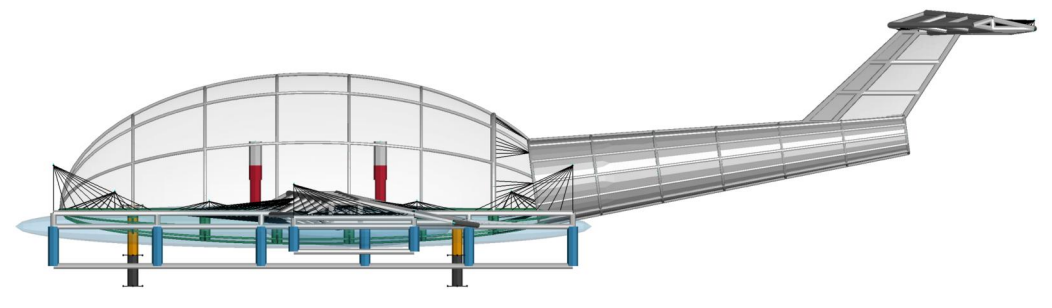
Figure 3b shows the landing gear crush absorber characteristics. The crush absorber triggers at 90% of the maximum oleo shock strut load and absorbs energy at 50% of the shock absorber load. The crush displacement is approximately 200 mm. As for the oleo strut characteristics, the landing gear crush absorber characteristics had to be adapted individually,



(a) High-wing configuration



(b) Mid-wing configuration



(c) Low-wing configuration

Figure 2. Positions of crushing absorbers (macro elements).

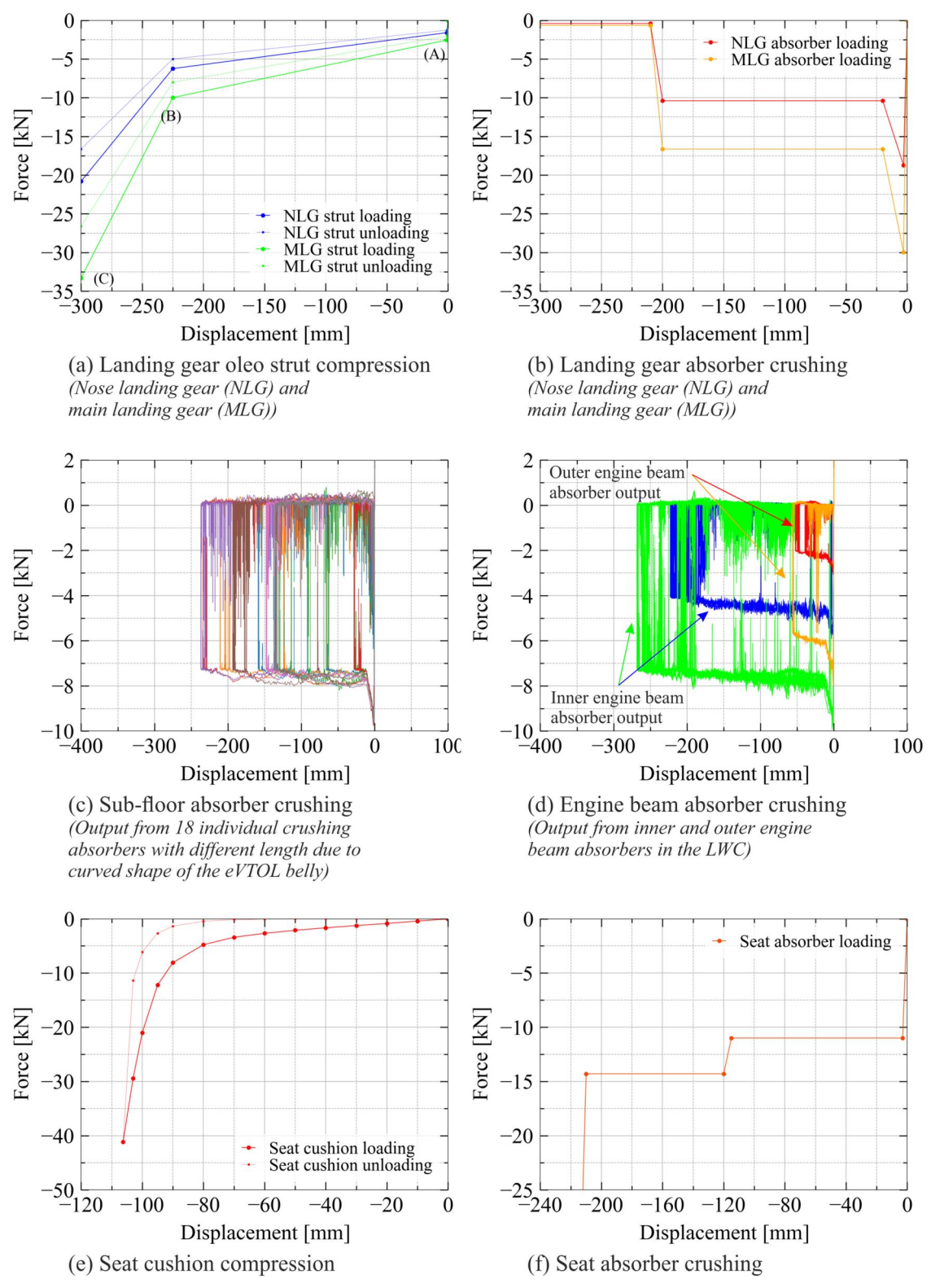


Figure 3. Connector input characteristics for energy absorbing devices (exemplary input for MWC).

depending on the centre of mass relative to the landing gear position.

In the HW-/MW-configuration, the main landing gear is attached to reinforced frames and additionally to the floor structure. In the LW-configuration, the main landing gear is attached to the inner engine beams and therefore defined without crush energy absorption capability. Here, the required energy

absorption capacity related to the landing gear is provided by crush absorber installations in the inner engine beams.

The sub-floor structure is modelled as a system of connector elements located underneath the cabin cross-beams that represent axial crushing according to typical force-displacement characteristics taken from literature [40], as shown in Figure 3c. Figure 3c shows force-displacement output from 18

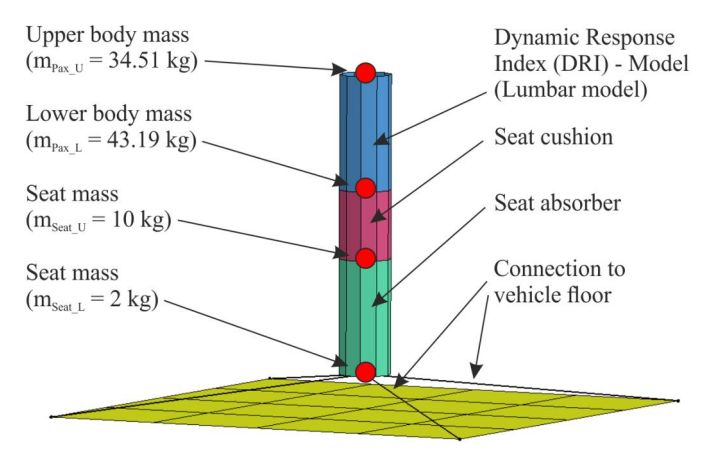


Figure 4. Simplified occupant-seat-model used in the simulation study.

individual sub-floor crush absorbers which have different length due to curved shape of the eVTOL belly. The same general crush characteristics were applied for the engine beam crush absorbers (Figure 3d). Figure 3d shows force-displacement output from 24 inner engine beam crush absorbers and 8 outer engine beam crush absorbers. Dependent on the wing configuration, the engine beam crush absorbers simply serve as load limiters for battery pack installations (HWC, MWC) or contribute to the vehicle crash energy management as the engine beam directly impacts the ground (LWC). The force plateau and displacement values depend on the position of the absorbers in the engine beam.

The occupant-seat-model consists of three connector elements which are connected in series (Figure 4). The lowest connector element represents the stroking seat absorber. The middle connector element represents the seat cushion and the upper connector element represents the occupant lumbar. The connector element representing the seat absorber is connected to the vehicle floor using the *CONSTRAINED INTERPOLATION function. The input characteristics for seat cushion and stroking seat absorber are shown in Figure 3e-f. The occupant is represented by the DRI model. The historical values for upper body mass m (34.51 kg), spring stiffness k (0.0966 kN/mm) and damping constant c (0.8181 kN*ms/mm) were estimated for U.S. Air Force pilots with a mean age of 27.9 years [35,36]. For older or younger population these constants are different [36]. In this context, using the DRI model to estimate the lumbar injury risk for UAM applications is a limitation as the above given input data for occupant modelling do not represent the wide range of our society. Also, the DRI model considers only purely vertical loading and is not capable to evaluate multi-axial occupant loading. Despite these limitations, the DRI model was chosen as it is a sufficient modelling approach for identification of trends in the conceptual design phase.

3.3. Crash energy absorption management

For the three considered wing configurations discussed in detail in Section 4 (HWC, MWC, LWC), different solutions

for the crash energy absorption management were developed and applied in the simulation study.

All considered energy absorption management solutions describe a systems approach of airframe crushing plus seat stroking. While airframe crushing is mainly designed to ensure structural integrity and hence for maintenance of survivable volume and emergency egress as well as for retention of mass items, seat stroking is designed to limit the occupant injury risk.

For the HW-configuration (Figure 2a) and the MW-configuration (Figure 2b), the wing structure is not directly involved in the ground impact in a crash event and hence does not contribute to the vehicle crash energy absorption. For this reason, the considered energy absorption management describes a crash cascade, with subsequent triggering of absorber stages, as follows:

- Airframe stage 1: Compression of landing gear oleo struts
- Airframe stage 2: Crushing of landing gear absorbers
- Airframe stage 3: Crushing of landing gear absorbers + sub-floor structure

For the LW-configuration (Figure 2c), the wing structure is directly involved in the ground impact in a crash event and hence contributes to the vehicle crash energy absorption. The considered energy absorption management describes a crash cascade, with subsequent triggering of absorber stages, as follows:

- Airframe stage 1: Compression of landing gear oleo struts
- Airframe stage 2: Crushing of (forward) landing gear absorbers + inner engine beams
- Airframe stage 3: Crushing of (forward) landing gear absorbers + inner engine beams + sub-floor structure

The LW-configuration is designed in a way that most of the vehicle's crash kinetic energy is absorbed by the inner engine beam absorbers. Due to the stiff wing-box structure, the available crush distance in the sub-floor area is limited wherefore the inner engine beams were designed to compensate that sub-floor limitation. Due to wing elastic bending, crushing of the inner engine beam significantly contributes to the global vehicle energy absorption, whereas the outer engine beam absorbers are designed as load limiters only, for protection of battery packs and power units.

For the LW-configuration, only the forward landing gear is equipped with a crash absorber, the rear landing gear is integrated in the engine beams and is defined without significant crush absorption capability as this function is provided by the engine beam structure.

Tables 2 and 3 summarise the available crush distances in each energy absorption area as well as the related mass involved in the individual crash cascade stage.

In Tables 2 and 3, the related mass of 1800 kg is the maximum take-off mass (MTOM) defined for this study.

Table 2. Available crush distances in each energy absorption area for HWC and MWC.

Energy absorption area	Crush distance (approximate values)	Related mass (kinetic energy to absorb)
Airframe stage 1): Compression of landing gear oleo struts	280 mm	1800 kg ¹
Airframe stage 2): Crushing of landing gear absorbers	120 mm	1800 kg
Airframe stage 3): Crushing of: landing gear absorbers + sub-floor structure	$80\mathrm{mm}+280\mathrm{mm}$	1800 kg
Seat: Crushing of seat absorbers	210 mm	87.7 kg ²

¹Mass of the entire vehicle.

Table 3. Available crush distances in each energy absorption area for LWC.

Energy absorption area	Crush distance (approximate values)	Related mass (kinetic energy to absorb)
Airframe stage 1): Compression of landing gear oleo struts	220 mm	1800 kg
Airframe stage 2): Crushing of: (forward) landing gear absorbers + inner engine beams	120 mm + 230 mm	1800 kg
Airframe stage 3): Crushing of: (forward) landing gear absorbers + inner engine beams + sub-	60 mm ¹	1800 kg
floor structure Seat: Crushing of seat absorbers	210 mm	87.7 kg

¹Crushing distance is limited due to the stiff wing box located in the sub-floor structure.

Table 4. Mass overview (exemplary for LWC).

Mass item	Mass		
Power units	8*50 kg = 400 kg		
Four occupants & four items of baggage	$4*77.7 \mathrm{kg} + 4*22.3 \mathrm{kg} = 400 \mathrm{kg}$		
Battery packs	400 kg		
Tail, rudder, elevator	150 kg (including distributed mass ¹)		
Wing, engine beams, engine mount	250 kg (including distributed mass)		
Fuselage	200 kg (including distributed mass)		
MTOW	1800 kg		

¹Due to the simplified modelling approach, portions of the structural mass are smeared over the model parts as distributed parts.

Table 4 provides further details on masses which contribute to the MTOM. These mass assumptions are based on [41] as well as on discussions with industry partners.

3.4. Further model and simulation details

A friction coefficient of $\mu = 0.3$ was used for self-contact and a friction coefficient of $\mu = 0.4$ was used for fuselage to impact surface interaction.

The selected nominal element size for the beam and shell elements is 45 mm, so that the Discretisation is capable of capturing global instability failure.

A full carbon composite eVTOL structure is assumed with different fibre orientation ratios for the fuselage structure and the wing structure. Material input data for the fuselage structure is based on assumed quasi-isotropic carbon fibre reinforced polymers (CFRP) composite laminates with fibre orientations [25/50/25], meaning that there are 25% 0° plies, 50% \pm 45° plies and 25% 90° plies. Material input data for the wing structure is based on assumed anisotropic CFRP composite laminates with fibre orientations [40/40/20]. Isotropic material stiffnesses were derived from these composite laminate assumptions and taken as input data for an isotropic elastic-plastic material model in LS-Dyna (*MAT_98/*MAT_SIMPLIFIED_JOHNSON_COOK) describing laminate failure by plastic yielding combined with 1% failure strain. The wing geometry was adjusted to match the geometrical moment of inertia of a wing profile provided by the industry partner.

A fully parameterised modelling and simulation approach was selected in this study. The FE meshes of all simulation models are generated using the Ansys parametric design language APDL (Ansys 19.2) and Python which enables fully parameterisation of eVTOL model generation including the FE mesh and LS-Dyna input files. The conversion of the FE mesh from the Ansys file format to the LS-Dyna file format was performed using a DLR in-house converter based on Python.

All explicit simulations were performed with LS-Dyna R10.2.0 on a computer cluster:

Operating System: Linux

CPU: Intel(R) Xeon(R) CPU E5540 @ 2.53 GHz

The simulations were performed on 1 node, with 8 CPU cores and using single precision. The calculation time for 300 ms simulation time was approximately 45 min.

The history data were recorded with an output frequency of 10 kHz and the field output data with an output frequency of 200 Hz. Nodal accelerations and forces were subsequently filtered with a Butterworth filter and a cut-off frequency of 180 Hz.

4. Finite element simulation study of different **eVTOL** configurations

This section presents the results of the performed simulation study on different eVTOL configurations using simulation models as described in Section 3.

²Mass of the occupant (77.7 kg) and the upper part of the seat (10 kg).

Section 4.1 discusses a first simulation run in which a wide range of different eVTOL configurations was simulated and assessed with the aim to identify most relevant key design parameters that may affect crashworthiness. Based on this assessment, three eVTOL configurations were selected for detailed analysis which is discussed in Sections 4.2-4.5.

4.1. First simulation run and selection of eVTOL configurations for detailed analysis

Based on a performed literature review on various eVTOL designs being proposed by the industry, several eVTOL 'lift + cruise' designs were selected with different characteristic vehicle architectures (Figure 5). Fundamental vehicle dimensions were derived from literature data [41] and transferred to the different vehicle architectures based on assumptions. Note that vehicle masses, specific design assumptions and material parameters used in the simulation study are discussed in Section 3. The range of eVTOL designs presented in Figure 5 is defined by several parameters: wing configuration, empennage configuration, position of battery packs and power units, the vehicle's centre of gravity, integration of the landing gear and position of the crash absorbers.

A first crash simulation run was performed for all eVTOL designs presented in Figure 5. The wing configuration was identified as the most crucial parameter that had a significantly higher influence on crashworthiness than all other parameters investigated in the first simulation run.

The main effects identified for the different wing configurations are:

- In a low-wing configuration, the stiff and hence noncrushable wing-box structure may limit the available crush distance in the sub-floor structure which can increase the crash loads and occupant injury risks.
- In a high-wing configuration, the wing is located above the cabin which requires reinforced frames to prevent cabin collapse and hence to maintain a survivable volume.
- In a mid-wing configuration, the wing can be placed behind the cabin so that the wing does neither affect the available sub-floor crush distance nor requires reinforced cabin frames to maintain survivable volume. Instead,



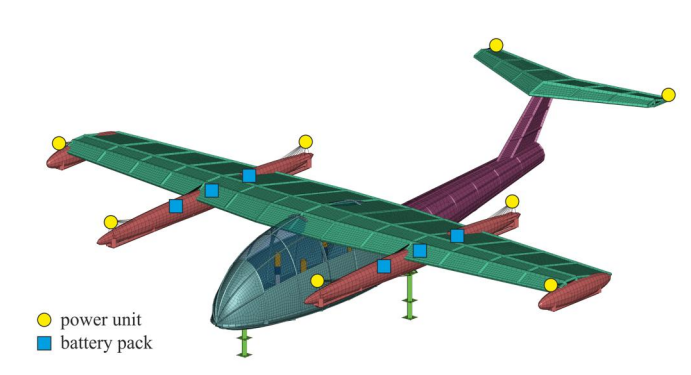
Figure 5. Range of investigated eVTOL designs.

cabin crushing under horizontal crash loading needs to be considered due to the heavy mass item behind the cabin.

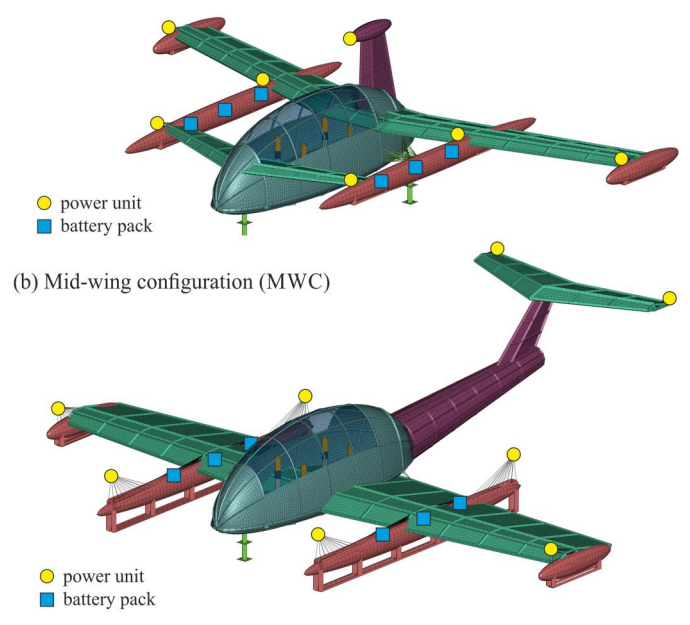
As an outcome of this first simulation run, the range of eVTOL configurations was narrowed down to three eVTOL concepts with different wing configuration as shown in Figure 6:

- a. High-wing configuration (HWC)
- b. Mid-wing configuration (MWC)
- c. Low-wing configuration (LWC).

These three configurations are further discussed in the following sub-sections. Thereby, the approach is to size the eVTOL structure and absorber devices mainly for the reference design load case (on-axis, $v_z=8\,\text{m/s}$) by taking into account sufficient reserve capacity and robustness (Section 4.2), and hereafter to evaluate key crashworthiness criteria for the on-axis, off-axis and real-world robustness load cases (Sections 4.3-4.5).



(a) High-wing configuration (HWC)



(c) Low-wing configuration (LWC)

Figure 6. eVTOL designs selected for detailed analysis.

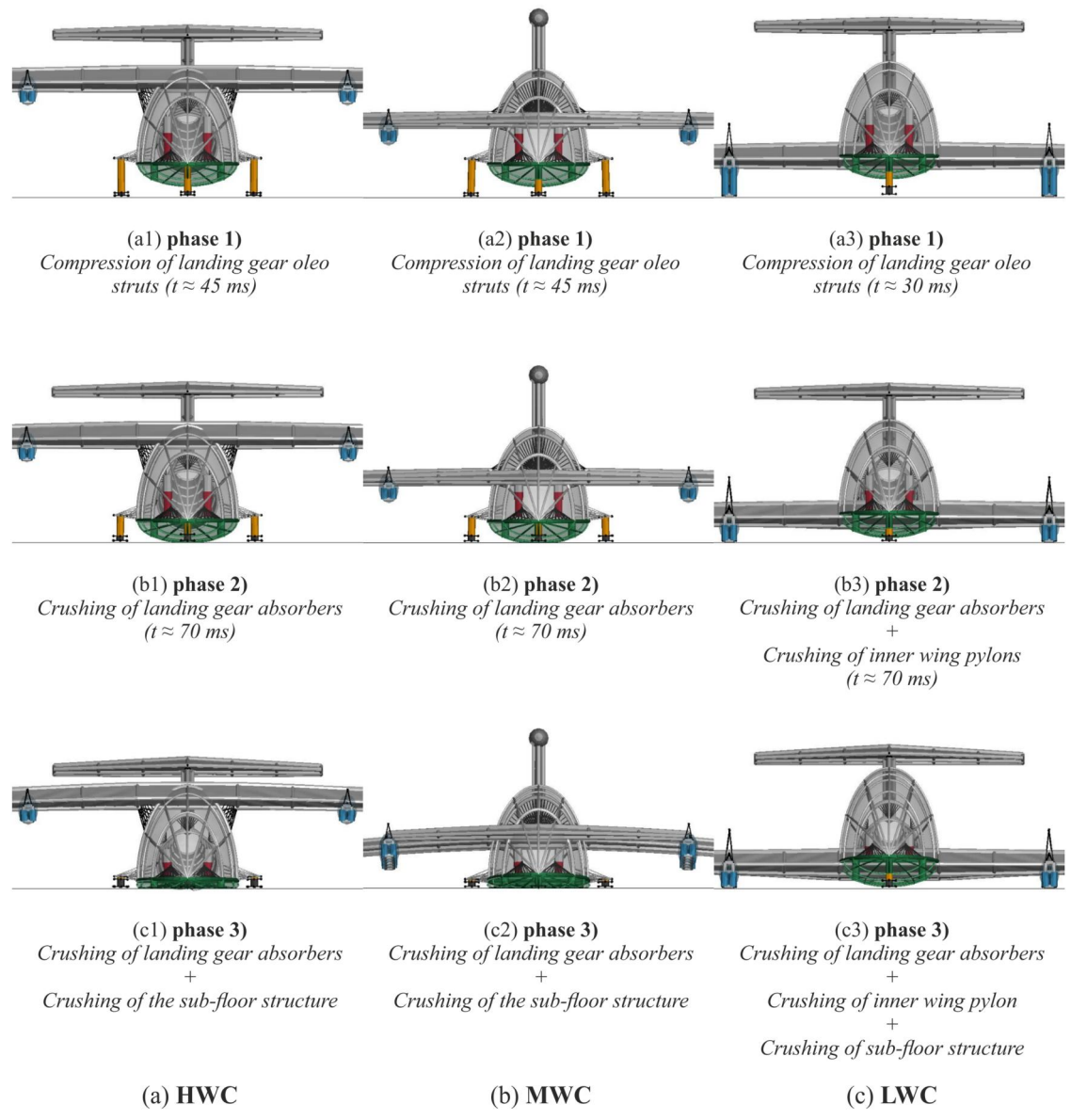


Figure 7. Crash sequence for the three selected eVTOL configurations. (reference design load case '#2').

4.2. Reference design load case with $v_z = 8 \text{ m/s}$ (on-axis, $v_x = 0 \text{ m/s}$)

This sub-section discusses the general energy absorption concept defined for the selected eVTOL configurations as presented in Figure 6. The characteristics of the individual crash absorbers were adjusted for each eVTOL configuration to obtain the desired crash kinematics and a favourable crash performance with smooth energy absorption throughout the crash sequence resulting in airframe structural integrity and acceptable occupant loads. Starting point for the adjustment of the crash energy absorbers in the sub-floor structure, engine beams, landing gears and seats is the reference design load case with a purely vertical impact velocity of $v_z = 8 \, \text{m/s}$ (load case '#2' in Table 1).

Figure 7 shows the crash sequence for the selected eVTOL configurations with HW-, MW- and LW-configuration. As described in Section 3.3, the crash sequence is

defined by a crash cascade. In the first phase, kinetic energy is absorbed by compression of the landing gear oleo struts. During the second phase, full compression of the landing gear oleo strut triggers the landing gear crush absorber, which is located in line with the oleo strut, and further kinetic energy is absorbed. For the LW-configuration, kinetic energy is additionally absorbed by crush absorbers in the inner engine beams. During the third phase, the sub-floor structure gets involved. For all three wing configurations, kinetic energy is absorbed in parallel by the landing gear crush absorbers and the sub-floor crush absorbers. For the LW-configuration, large portions of the kinetic energy are absorbed by additional crush absorbers in the inner engine beams which compensate the limited sub-floor crush distance under the stiff low-wing structure.

Figure 8 shows plots of overall energy curves for all three eVTOL configurations, where E_{total} is the total energy, $E_{kin}^{t_0}$ is the initial kinetic energy, W_{ext} is the external work of the



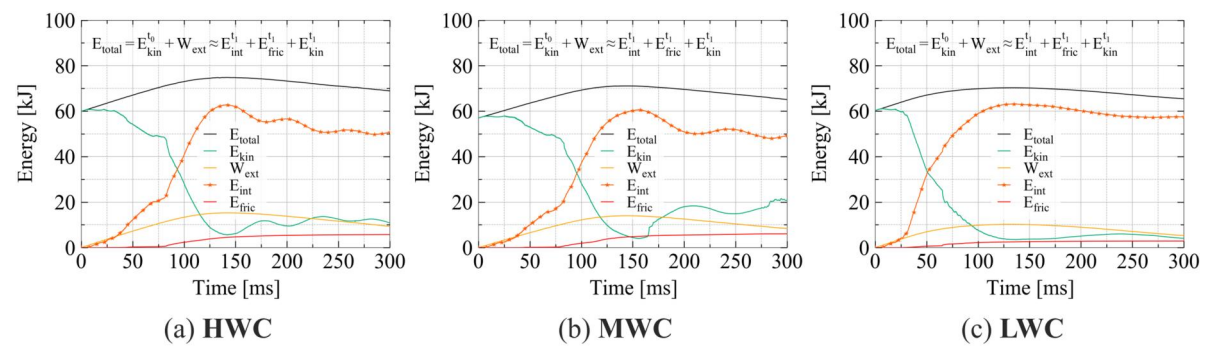


Figure 8. Overall energy plot (reference design load case '#2').

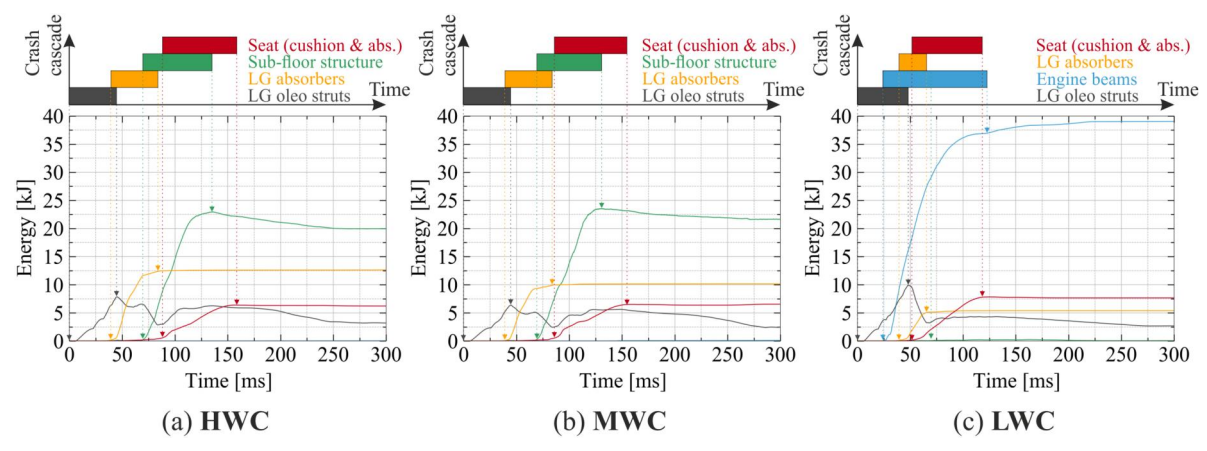


Figure 9. Energy absorption in the individual structural regions (reference design load case '#2').

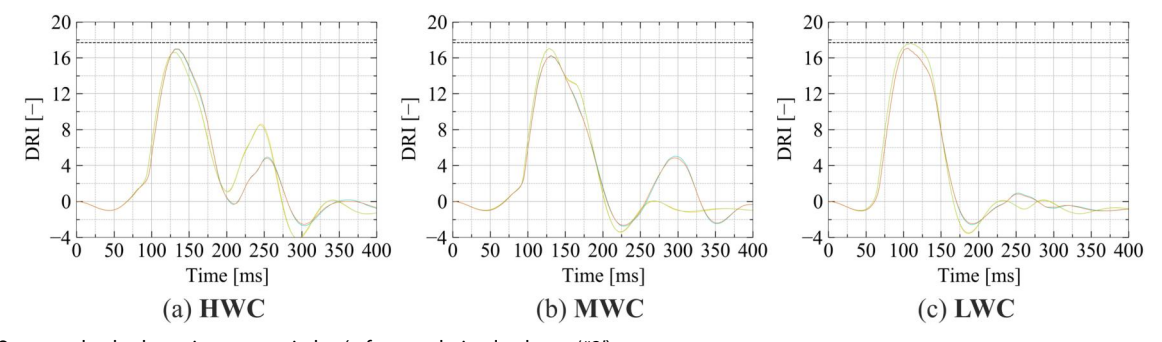


Figure 10. Occupant loads: dynamic response index (reference design load case '#2').

gravity field, $E_{int}^{t_1}$ is the current internal energy, $E_{fric}^{t_1}$ is the current frictional dissipated energy and $E_{kin}^{t_1}$ is the current kinetic energy. The main crash impact shows durations of 125-150 ms, with subsequent rebound of the vehicle for t > 125-150 ms. The triggering of the individual crash cascade phases can clearly be seen by unsteadiness in the plots of internal energy respectively kinetic energy. This is a typical characteristic for a crash cascade concept as with each cascade level the crash load and hence the slope of the internal energy curve increases. Comparing the internal energy curves of all three charts in Figure 8 reveals similar crash characteristics for the HW- and MW-configuration with stepwise increasing energy absorption (increasing slope of curve) while for the LW-configuration the second cascade level provides already a high-energy absorption rate (steep slope of curve). This comparably stiff response of the LW-

configuration is required due to the limited crush distance below the stiff wing and hence caused by the engine beam crushing which is designed to correspondingly higher load levels. This circumstance is shown in more detail in Figure 9 which shows the energy absorption in the individual structural regions for the HW-, MW- and LW-configuration. For the HW- and MW-configuration, most of the kinetic energy is absorbed in the sub-floor structure, while for the LW-configuration the engine beams absorb most of the kinetic energy and hence compensate the limited subfloor crush distance.

Figure 10 considers the occupant injury risk and compares plots of DRI-time curves for each occupant, showing charts for the HW-, MW- and LW-configuration. The presented DRI values are based on the nodal accelerations taken from the occupant-seat model. For all three wing configurations,

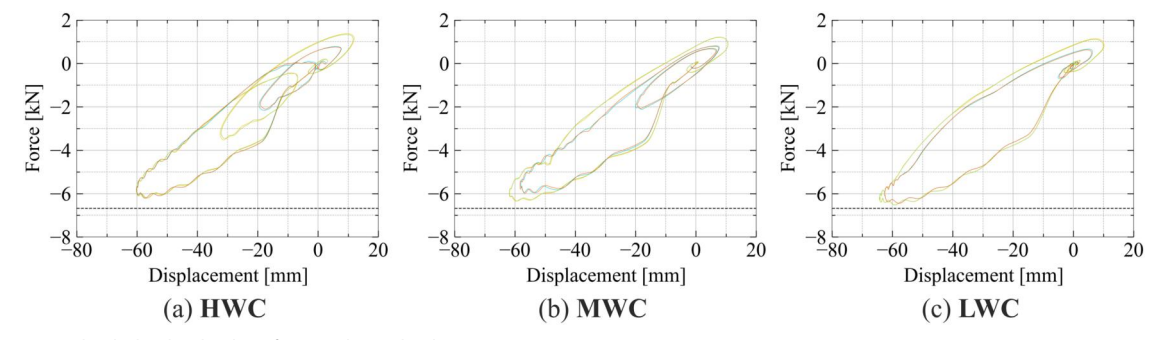


Figure 11. Occupant loads: lumbar loads (reference design load case '#2').

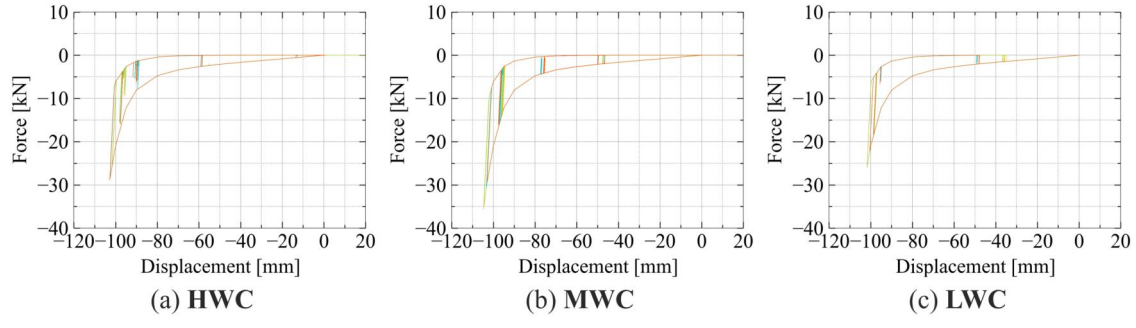


Figure 12. Seat cushion: Force-displacement beam element output.

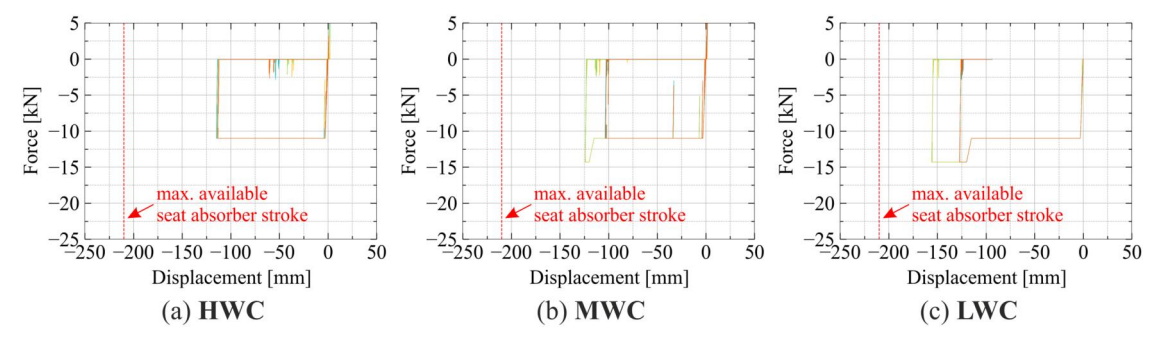


Figure 13. Stroking seat absorber: Force-displacement beam element output.

similar maximum DRI values are obtained, although for the LW-configuration the DRI maximum is reached at $t \approx 105$ ms and thus 25 ms earlier compared to the HW- and MW-configurations. Hence, the stiffer airframe response for the LW-configuration, as indicated in the energy plots in Figure 8, is compensated by the seat stroke, leading to similar maximum occupant loading, although the time of maximum occupant loading is accordingly different. The dashed line in the charts of Figure 10 represents a DRI value of 17.7 which is the injury risk limit selected for this study. According to [35], a DRI value of 17.7 leads to a 10% spinal injury probability. In addition to the assessment of DRI values, the occupant-seat model was also used to analyse the compression forces in the human lumbar, between upper body and pelvis node. Figure 11 compares the compression-force output of the beams representing the human lumbar in the DRI model. The dashed line in the charts of Figure 11 represents a compressive lumbar load of 6674 N according to the certification requirements stated in EASA CS27.562(c)(7).

The seat data are presented in Figures 12 and 13. Figure 12 compares the force-displacement output of the beams representing the seat cushion in the occupant-seatmodel. The output follows the defined input characteristics shown in Figure 3c. Figure 13 compares the force-displacement output of the beams representing the stroking seat absorbers in the occupant-seat-model. As desired, for this reference design load case, the seat stroke absorbers provide sufficiently residual energy absorption capacity and hence robustness against more severe crash load cases: For the HW-configuration and the MW-configuration about 54% respectively 59% of the seat absorbers' capacity is utilised. For the LW-configuration, the compensation of the comparably stiff airframe response led to a significantly higher stroke of about 74% of the seat absorbers' capacity. As a result, there is less reserve stroke capacity available for the LW-configuration, which leads to a higher risk of bottoming-out effects and hence occupant injuries in more severe crash load cases.

4.3. Crashworthiness evaluation for varying vertical impact energies

A well-defined energy absorption management must ensure crash safety for varying crash impact conditions up to, and beyond, the reference design load case. Impact conditions with reduced impact energy must be considered due to the risk of stiff airframe response as lower crash loads may not lead to triggering of the crash absorbers. Furthermore, a certain extrapolation beyond the reference design load case shall ensure robust crash safety concerning more severe impact conditions without obtaining bottoming-out or other failure effects that lead to an abrupt change of the crash performance. Both is considered in this sub-section with the vertical impact conditions of $v_z = 4 \text{ m/s}$ (load case '#1') and $v_z = 10 \text{ m/s}$ (load case '#3') as shown in Table 1.

This sub-section compares the reference design load case with the robustness load cases $v_z = 4 \,\text{m/s}$ and $v_z = 10 \,\text{m/s}$ based on three key crashworthiness parameters:

- Maintenance of acceptable acceleration loads experienced by the occupants
- Retention of heavy items of mass: battery pack and power units
- Maintenance of survivable volume

Other key crashworthiness parameters, such as emergency egress path and post-crash hazards, are not considered here.

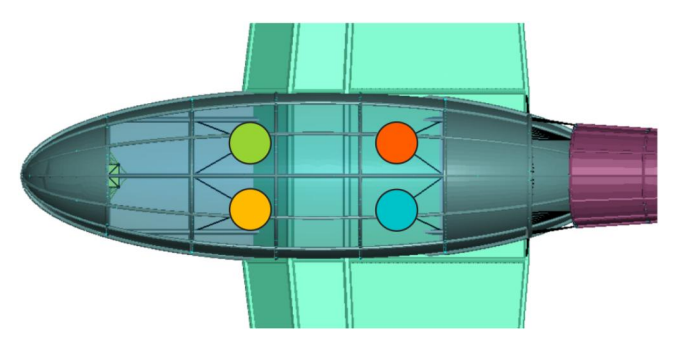


Figure 14. Occupant positions in the cabin (top view).

4.3.1. Maintenance of acceptable acceleration loads experienced by the occupants

Figure 14 shows the top view of the eVTOL cabin with the positions of the four occupants highlighted in different colours which corresponds to the bar diagram of DRI values shown in Figure 15.

Figure 15 shows plots of bars with maximum DRI values reached for each occupant in the three different eVTOL configurations, for the reference design load case and both robustness load cases. For the reference design load case (vz = 8 m/s), the DRI values of each eVTOL configuration are similar and below the critical DRI value of 17.7, an outcome previously discussed in Section 4.2.

For the low-energy robustness load case with $v_z = 4 \text{ m/s}$, the HW- and MW-configurations show significantly lower DRI values compared to the LW-configuration. Again, the comparably stiff airframe response of the LW-configuration, required due to limited crush distance below the wing structure, shows an influence leading to DRI values close to the limit of 17.7 even for low-energy crash impacts. However, the DRI values are still below the critical DRI value of 17.7.

For the high-energy robustness load case with $v_z = 10 \text{ m/}$ s, the impact kinetic energy is approx. 56% higher compared to the reference design load case ($v_z = 8 \text{ m/s}$). For the HWand MW-configurations, the stroking seat absorber provides sufficient energy absorption capacity leading to DRI values that only slightly exceed the limit of 17.7. In contrast, for the LW-configuration the stiff airframe response led already for the reference design load case to a higher seat stroke consumption so that here for the high-energy robustness load cases the seat stroke is used up leading to bottomingout effects and clear exceeding of the DRI limit of 17.7. Figure 16 shows the seat stroke for the high-energy robustness load case ($v_z = 10 \text{ m/s}$), the bottoming-out effect for the LW-configuration (Figure 16c) can clearly be seen. For the HW-configuration (Figure 16a), the plot of curves indicate that the available stroke was fully used up showing initial bottoming-out.

4.3.2. Retention of items of mass (battery packs and power units)

The key crashworthiness parameter 'retention of items of mass' is assessed with regard to the propulsion system masses: battery packs and power units. The vertical

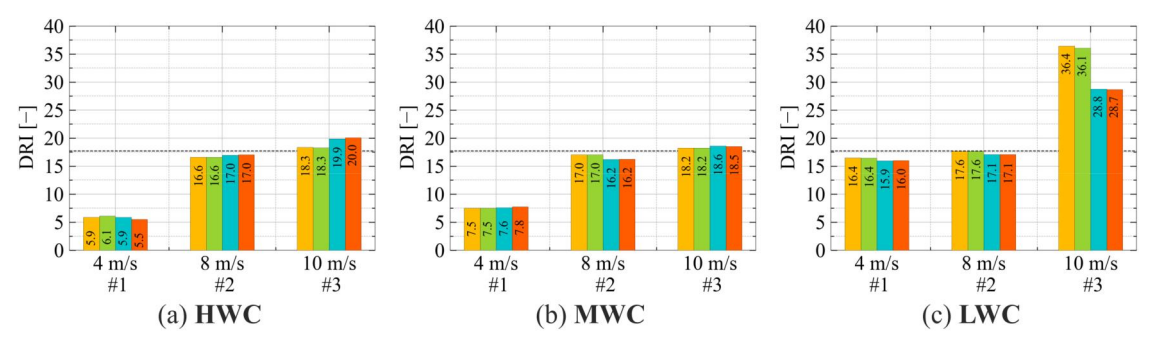


Figure 15. Occupant loads: Dynamic response index (colours refer to Figure 14).

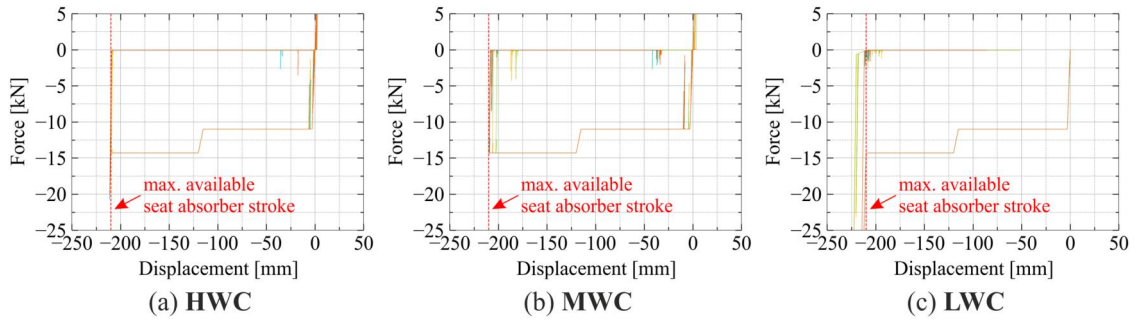
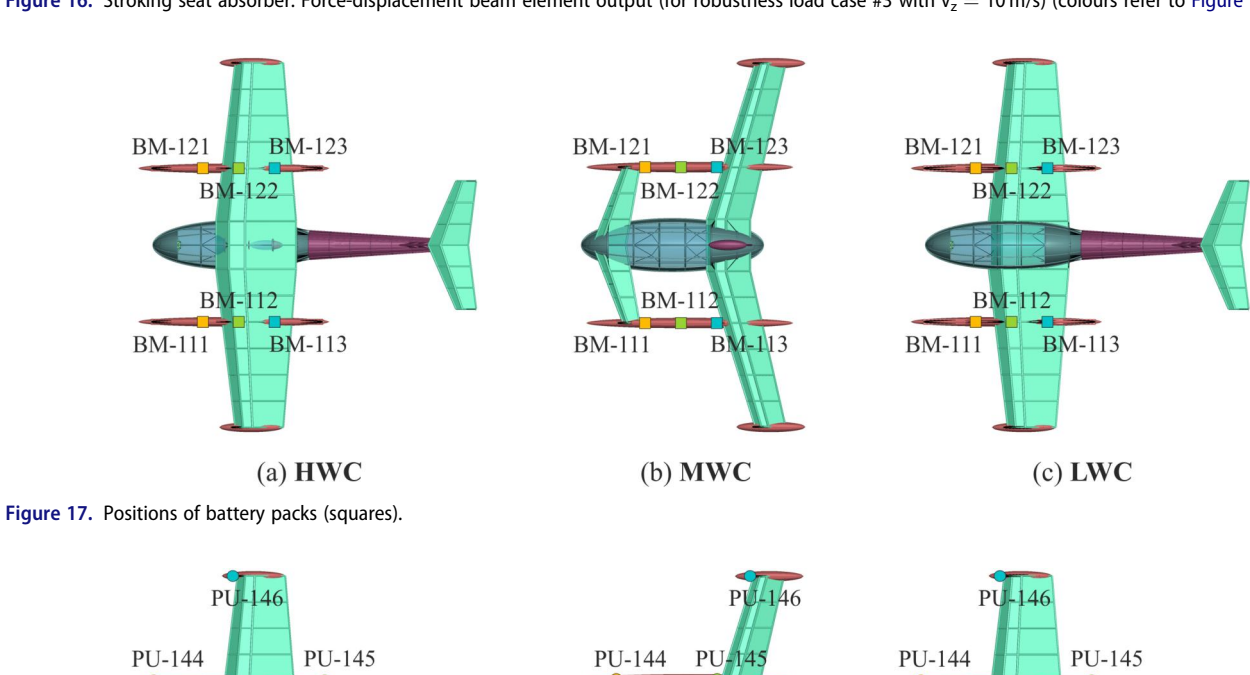


Figure 16. Stroking seat absorber: Force-displacement beam element output (for robustness load case #3 with v_z = 10 m/s) (colours refer to Figure 14).



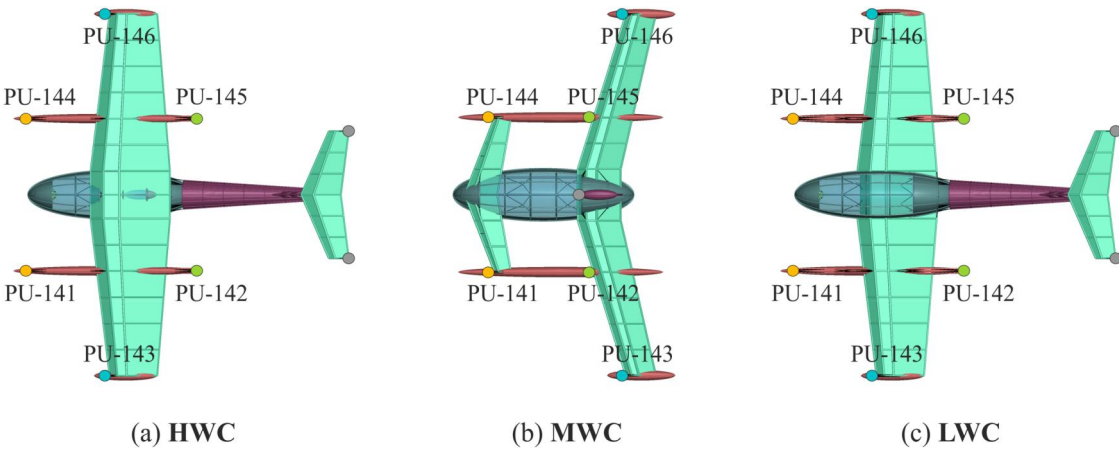


Figure 18. Positions of power units (circles).

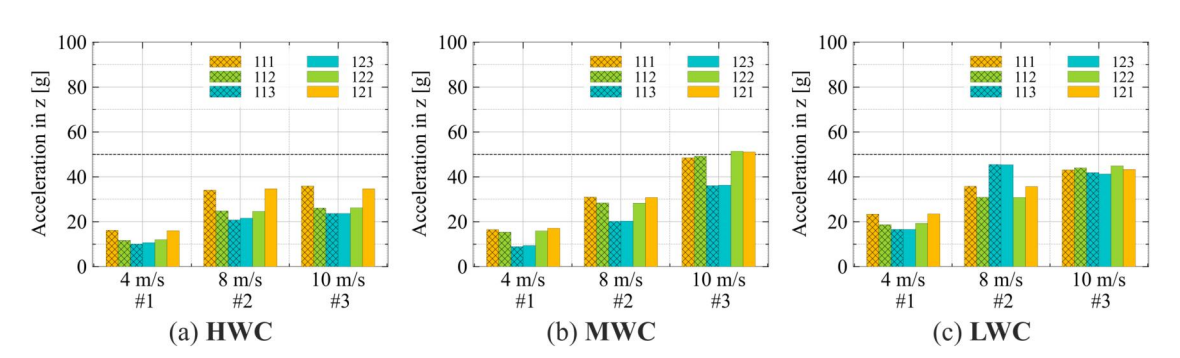


Figure 19. Retention of items of mass (battery pack max. vertical acceleration). (colours refer to Figure 17).

accelerations measured at the single mass elements are used for the assessment. Figure 17 shows the positions of battery

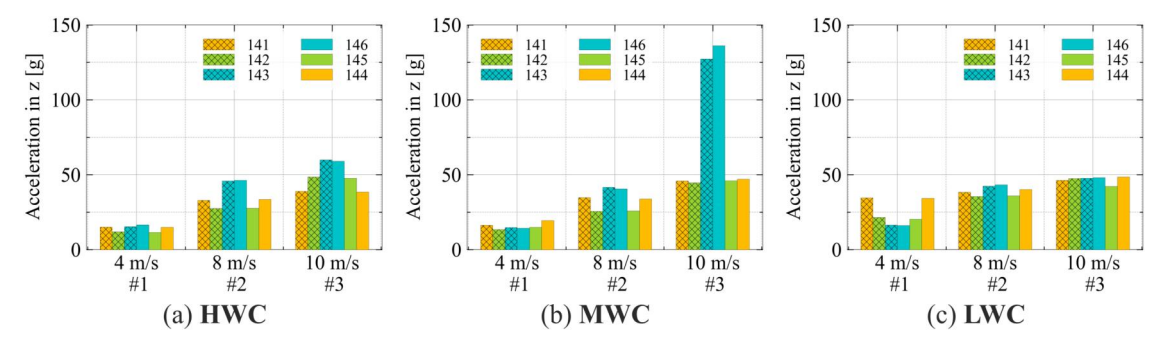


Figure 20. Retention of items of mass (power unit max. vertical acceleration). (colours refer to Figure 18).

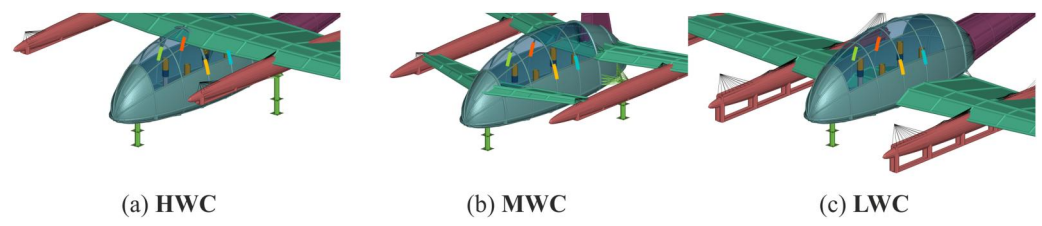


Figure 21. Positions of frames used for evaluation of survivable volume (highlighted in colour).

packs which are distributed in the inner engine beam for all three considered eVTOL configurations. Figure 18 shows the positions of power units at the inner and outer engine beams as well as at the horizontal stabiliser.

Figure 19 compares the vertical accelerations of the battery pack mass elements for the three eVTOL configurations (HWC, MWC and LWC), with $v_z = 4 \text{ m/s}$, $v_z = 8 \text{ m/s}$ and $v_z = 10 \,\mathrm{m/s}$. The dashed line in the charts represents an assumed limit of 50 g for the battery packs which should not be exceeded for the considered load cases of this study. According to [42], the maximum acceleration load of a battery pack should not exceed a threshold value of 50 g to reduce risk of fire during or after a crash landing. The energy storage crashworthiness approach considered in this study intends to prevent a battery thermal runaway under emergency landing conditions, but allows exceeding of acceleration allowables and hence allows contained thermal runaway under survivable emergency landing conditions.

Figure 20 compares the vertical accelerations of the power units, for the three eVTOL configurations (HWC, MWC and LWC), with $v_z=4\,\text{m/s},\ v_z=8\,\text{m/s}$ and $v_z=$ 10 m/s.

For both mass retention categories, battery packs and power units, the same trend can be identified. The HWand MW-configurations were expected to experience no direct ground contact in case of a crash event, which is why their engine beams were not designed with corresponding load limiters for the battery pack and power unit installations. In contrast, the LW-configuration was expected to experience direct ground contact and the engine beams were designed for both, to absorb significant portions of the vehicle's kinetic energy and to limit the accelerations for the battery packs and power units. The simulation results in Figure 19 and Figure 20 show acceptable accelerations for all three eVTOL configurations despite direct ground contact for the LW-configuration, hence the engine beam load limiters for the LW-configuration were properly designed. As an exception, the high-energy load case ($v_z = 10 \text{ m/s}$) for the MW-configuration shows high battery pack accelerations close to the limit of 50 g and significantly higher accelerations for the power units at the outer engine beam. For the MW-configuration, the impact condition with $v_z = 10 \,\text{m/s}$ led to wing deformation and a direct ground impact of the outer engine beams. As for this MW-configuration, load limiters in the outer engine beams were not designed for direct ground impact, the corresponding power units experienced high accelerations. This effect exemplarily clarifies, how local load limiters can significantly improve the crash design and prevent mass items from coming loose.

4.3.3. Maintenance of survivable volume

The key crashworthiness parameter 'maintenance of survivable volume' is assessed with regard to the cabin volume and the risk of main frame failure. The axial forces measured in the main frame beam elements were used for the assessment. Figure 21 shows for the HW-, MW- and LWconfigurations the positions of the frames which were evaluated. For the HW-configuration, these are the reinforced main frames which support the wing. For the MW- and LW-configurations, these frames are of filigree design due to the absence of overhead masses, but they are located in the simulation models at the same positions as in the HWconfiguration and hence enable a direct comparison.

Figure 22 shows plots of bars representing the maximum axial frame forces for the three eVTOL configurations (HWC, MWC and LWC), with $v_z = 4 \,\text{m/s}, \, v_z = 8 \,\text{m/s}$ and $v_z = 10 \,\text{m/s}$. In general, the max. axial frame forces for the HW-configuration are considerably higher compared to the

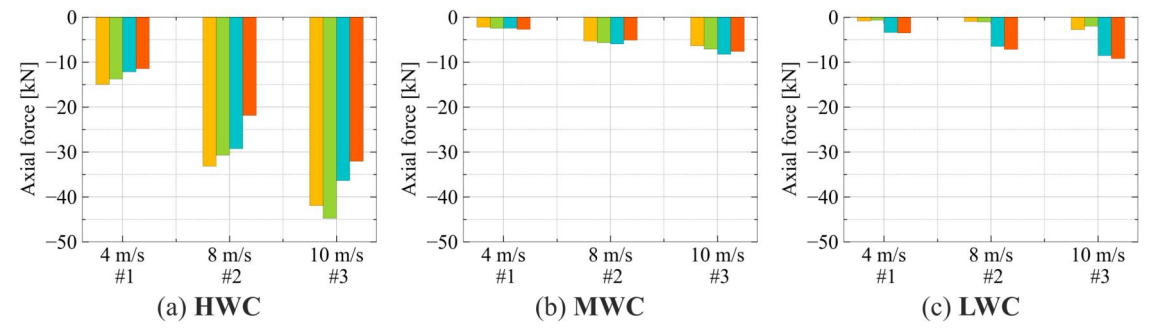


Figure 22. Maintenance of survivable volume (maximum axial force in the frames). (colours refer to Figure 21).

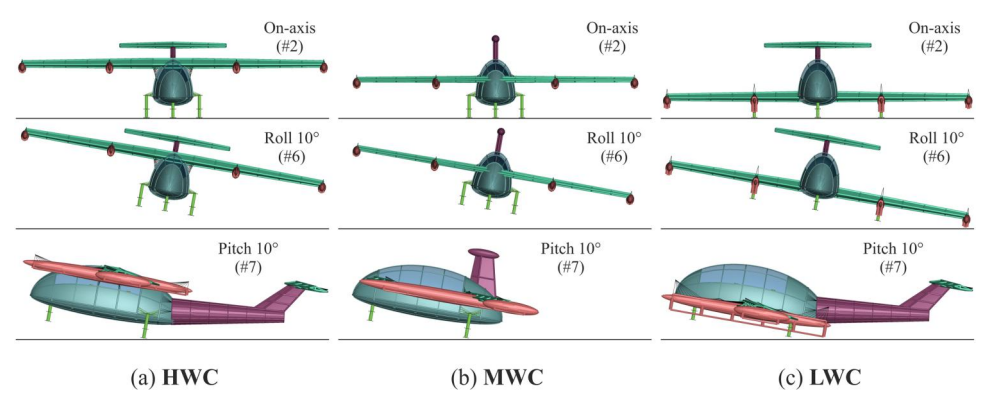


Figure 23. Initial impact conditions for varying off-axis attitudes ($v_z = 8 \text{ m/s}$).

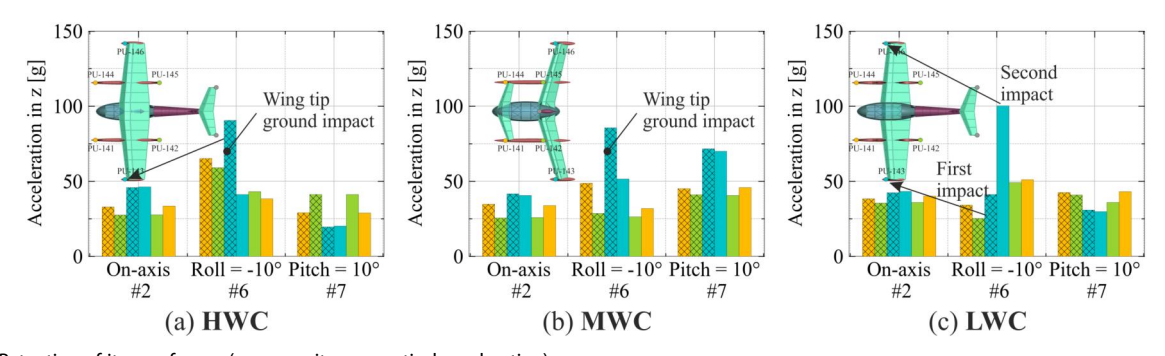


Figure 24. Retention of items of mass (power unit max. vertical acceleration). (colours refer to Figure 18).

MW- and LW-configuration, due to the high-wing mass inertia. The comparison of frame loads in Figure 22 clearly highlights the risk of cabin collapse for high-wing configurations and the need for a massive frame design.

4.4. Crashworthiness evaluation for varying off-axis impact attitudes

This sub-section discusses the simulation results of the off-axis robustness load cases with purely vertical impact velocity of $v_z = 8$ m/s, as shown in Table 1. The reference design load case '#2' is compared with load case '#6', with a roll angle $\varphi = 10^\circ$, and load case '#7', with a pitch angle $\theta = 10^\circ$. Figure 23 shows the initial impact conditions of the

three load cases considered in this sub-section, for the three eVTOL configurations.

In this sub-section, only the key crashworthiness parameters 'retention of items of mass' and 'survivable volume' are discussed to highlight main effects caused by off-axis impact attitudes.

4.4.1. Retention of items of mass (battery packs and power units)

Two main effects were identified with regard to the mass retention criterion. First, off-axis impact attitudes may lead to direct ground contact of structural regions that were not expected therefor and hence not designed for direct ground impact. Second, off-axis attitudes may lead to an asymmetric first impact resulting in rotation of the aircraft and a second

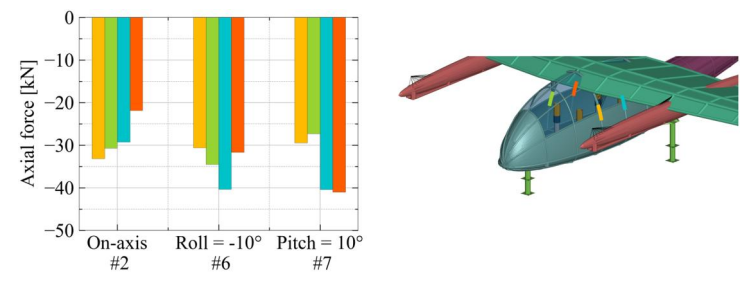


Figure 25. Maintenance of survivable volume in the HW-configuration. (evaluation of max. axial force in the frames).

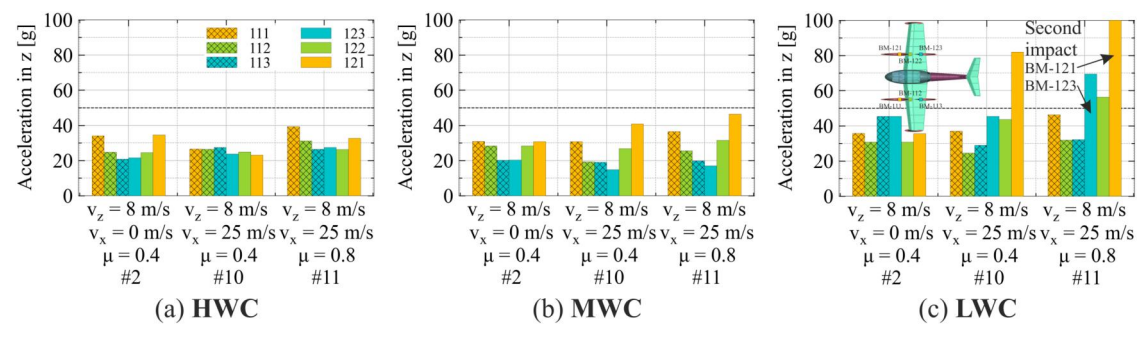


Figure 26. Retention of items of mass (battery pack max. vertical acceleration). (colours refer to Figure 17).

impact at the opposite aircraft location, which can sometimes result in significantly higher local impact velocities compared to the first impact. Both effects are shown in the following based on the power unit accelerations.

Figure 24 compares the vertical accelerations of the power units for the three eVTOL configurations (HWC, MWC and LWC). The HW- and the MW-configurations show significantly higher power unit accelerations for an impact attitude with roll angle 10° compared to on-axis impact. The off-axis impact condition with roll angle led to direct ground contact of the left wing-tip with an outer engine beam not designed for direct impact and hence not equipped with load limiters. For this reason, the power unit in the outer left engine beam experienced accelerations of more than 75 g resulting in the risk of breaking loose and becoming a hazardous projectile. The LW-configuration is designed for engine beam ground impact and hence the power units in the engine beams are equipped with load limiters. Despite that, the chart in Figure 24 shows high power unit accelerations for the LWconfiguration impact condition with a roll angle of 10°. While the first impact occurred on the left wing-tip with an engine beam load limiter designed for this loading condition, the aircraft subsequently rotated by the first impact impulse leading to a second impact at the right wing-tip with significantly higher local impact speed that exceeded the power unit load limiter capacity. The power units in the right engine beam experienced accelerations of more than 100 g, again resulting in the risk of breaking loose and becoming a hazardous projectile.

This discussion of simulation results reveals the importance to consider off-axis impact conditions in the design process to ensure proper design of local energy absorbers.

4.4.2. Maintenance of survivable volume

One main effect was identified with regard to the survivable volume criterion. Off-axis impact conditions generally result in asymmetric structural loading, which may end up in increased frame loads and hence higher risk of cabin collapse.

Figure 25 shows plots of bars representing the main frame axial loads for the three considered load cases and the HW-configuration. Asymmetric frame loading can be seen for both off-axis load cases with increased frame loads compared to the on-axis reference design load case.

4.5. Crashworthiness evaluation for varying combined vertical/horizontal impact velocities

This sub-section discusses the simulation results of load cases with combined vertical/horizontal impact velocities and the influence of the friction coefficient as shown in Table 1 for the load cases '#9' - '#14'. Only selected load cases are discussed to highlight the main outcomes. These are the reference design load case '#2' compared with load cases '#10' and '#11', both representing non-zero roll ($\varphi =$ -10°), pitch ($\theta = 10^{\circ}$) and yaw ($\psi = -10^{\circ}$) angles, as expected for real-world crash events. In addition, load case '#11' considers an increased friction coefficient between aircraft and ground of $\mu = 0.8$ to consider in a simplified and efficient way increased longitudinal crash loads introduced in case of soft soil impact terrain.

In this sub-section, only the key crashworthiness parameters 'retention of items of mass' and 'survivable volume' are discussed to highlight main effects caused by real-world crash impact conditions.

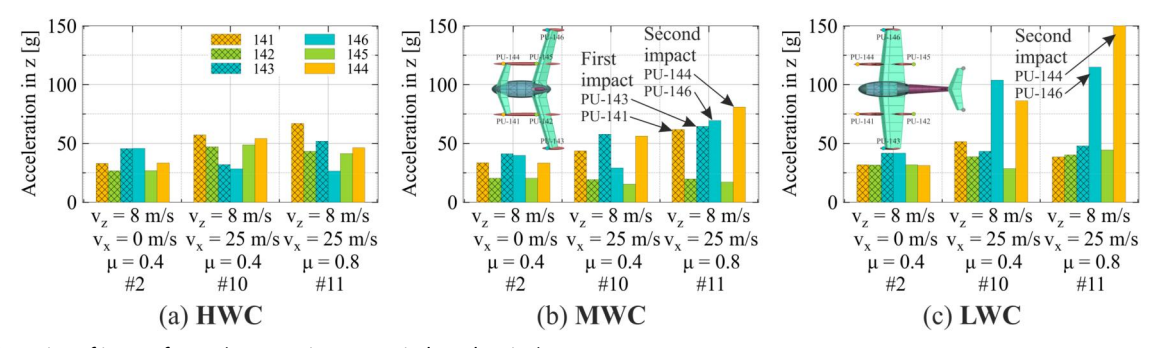


Figure 27. Retention of items of mass (power unit max. vertical acceleration). colours refer to Figure 18).

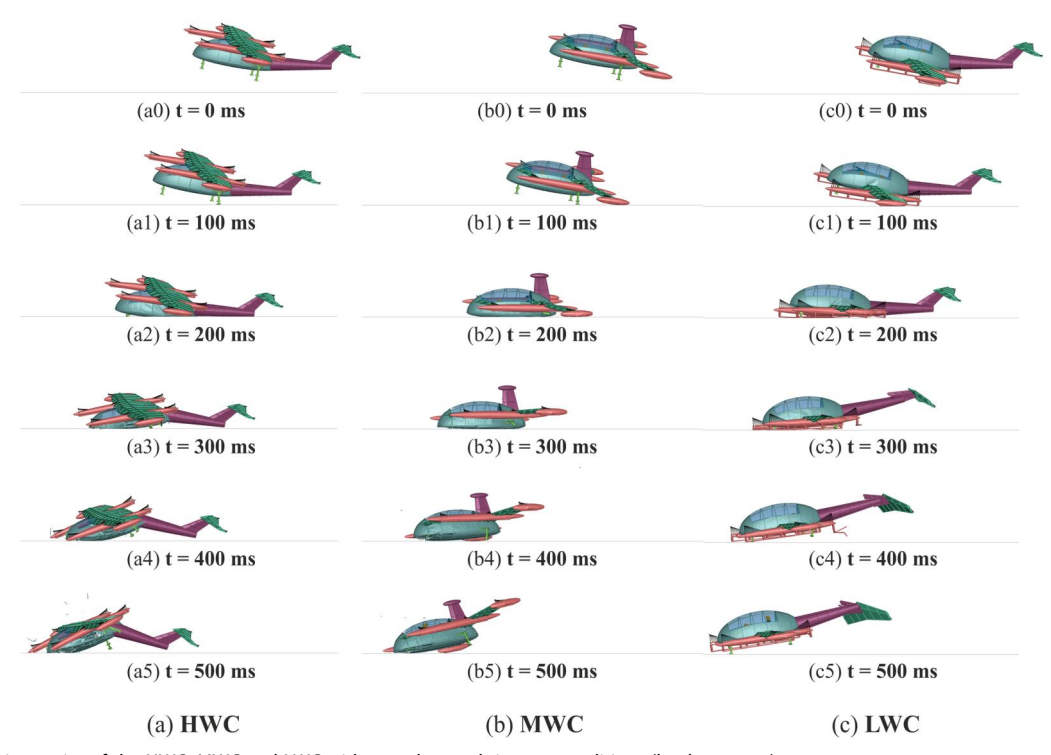


Figure 28. Crash kinematics of the HWC, MWC and LWC with complex crash impact conditions (load case #11).

4.5.1. Retention of items of mass (battery packs and power units)

Vertical accelerations of the battery packs (Figure 26) and power units (Figure 27) are compared for the three eVTOL configurations. Dependent on the wing configuration, the mass item accelerations show less (HWC) or more distinct (LWC) influence of the load case complexity on the resulting mass item accelerations. Based on these simulation results, it can be assumed that mass item installations in a high wing are better protected from severe impact loads, while mass item installations in a low wing may experience such high crash loads under real-world crash impact conditions that any attempt of mass retention may fail. In this context, the simulation results presume structural integrity of the wing and hence potential wing rupture under the vertical impact loads is not considered.

Figure 28 presents the crash kinematics for load case '#11', simulated with increased friction of $\mu=0.8$, comparing the HW-, MW- and the LW-configuration. The crash sequence of the LW-configuration clearly shows the distinct

ground interaction of the engine beams as well as the first impact on the left wing-tip with subsequent aircraft rotation and second impact at the right wing-tip. The crash sequence of the HW-configuration shows distinct ground interaction with the airframe fuselage while the upper wing is less distinctly involved in ground interactions. In contrast to the LW-configuration, a more distinct rollover tendency can be seen which is driven by the high-wing mass inertia and which resulted in disintegration of the tail boom.

4.5.2. Maintenance of survivable volume

Figure 29 shows the evaluation of axial forces in the main frames as described in Section 4.3.

A clear trend for the HW-configuration can be derived from Figure 29, showing significantly increased loads in the main frames for real-world crash impact conditions compared to the purely vertical design load cases. Especially for the HW-configuration, introducing the horizontal velocity component combined with increased friction leads to shear

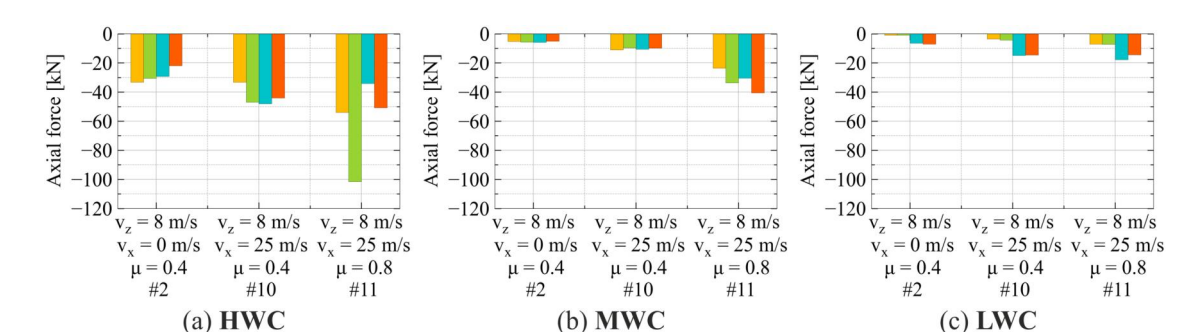


Figure 29. Maintenance of survivable volume (evaluation of max. axial force in the frames). (colours refer to Figure 21).

loading of the airframe structure and to significantly higher axial forces in the main frames. This is a reasonable trend considering the mass inertia of the high-wing that introduces large moments in the fuselage leading to compression loading of the forward main frames. For the HW-configuration, the forward main frame did fail which resulted in partial collapse of the cabin. There is a clear risk of cabin collapse which becomes more relevant under real-world impact conditions. Hence, concerning the maintenance of survivable volume, significantly better robustness under real-world impact conditions can be expected for the LW-and MW-configurations.

5. Conclusions

This paper presents a crashworthiness evaluation of three selected eVTOL configurations in an early conceptual design phase. A simplified macro-FE modelling approach is used and the performed simulations consider crash load cases with aspects from real-world accident scenarios to ensure robust crash safety in the design process. In this context, only load cases of 'emergency landing' category are considered, which aim at providing the occupants every reasonable chance of escaping serious injuries [43].

5.1. General conclusions that can be drawn from the presented research results are

- The selected macro-FE modelling approach in combination with an automated and parameterised finite element modelling could be confirmed as an advantageous simulation approach for conceptual design studies.
- The consideration of a wider range of crash impact conditions that align with real-world accident scenarios can reveal shortcomings in the design, as effects may occur which are not covered by typical crash design load cases of purely vertical impact with on-axis aircraft attitude. As examples: Off-axis impact attitudes may lead to asymmetric loading conditions with second impacts showing a significantly higher local impact velocity compared to the initial impact speed. Combined vertical/horizontal crash impact conditions may lead to significantly different structural loading compared to purely vertical conditions which may require specific crash sizing or even the

- rejection of an aircraft design due to unfavourable fundamental crash performance under real-world crash conditions.
- Main trends identified in the crashworthiness evaluation of the considered eVTOL configurations correspond to the crash behaviour known from traditional small aeroplanes, e.g. the crucial effect of the wing configuration on crash safety. But in contrast to traditional small aeroplanes, it is expected that eVTOLs with a 'lift+cruise' configuration, typically equipped with engine beam installations, are expected to be more prone to detach mass parts, as heavy mass installations are distributed throughout the aircraft.
- On the basis of the performed simulations, most favourable crash performance could be identified for the MW-configuration. The wing can be placed behind the cabin without affecting the available sub-floor crush distance (as for the LW-configuration) and without affecting the frame sizing to maintain survivable volume (as for the HW-configuration). Solely, cabin crushing under horizontal crash loading needs to be considered due to the heavy mass item behind the cabin.
- The results obtained in the discussed simulation study were used to identify trends rather than absolute values. Considering the simplified modelling approach and the lack of experimental data, the presented purely numerical approach has been identified as well suited for conceptual design studies, with the focus on identification of trends. Further progress in the design towards preliminary and detail design levels would require model validation based on experimental data.

5.2. Specific conclusions that can be drawn from the presented research results are

- Critical items should be installed close to the aircraft centre as outer regions may experience high local impact loads under real-world crash conditions. In this context, battery packs and power units installed in engine beams need to be properly integrated to prevent them from breaking loose or becoming a post-crash hazard, e.g. due to battery thermal runaway in the evacuation path.
- Local load limiters installed at mass items can significantly improve the crash design and prevent mass items from breaking loose and becoming a hazardous projectile. Those load limiters should be

- designed for local impact speeds that may be significantly higher than the considered vehicle crash impact velocities.
- installed also in structural regions where direct ground impact is not expected but may occur under real-world crash conditions.
- The seat stroke design should consider the true airframe crush performance. An extended available seat stroke may significantly improve crash survivability as bottoming-out effects and hence a high injury risk can be prevented even under real-world crash conditions, enabling the occupants to evacuate themselves. The simulation results showed seat stroke exceedance for stiff airframe response and real-world crash conditions.
- Main frame design for HW-configurations should consider high shear loads introduced by the high wing in case of combined vertical/horizontal impact conditions and leading to high risk of cabin collapse.

Acknowledgements

Parts of the research leading to these results were accomplished in the framework of the 5th Aeronautical Research Program of the German Federal Ministry of Economic Affairs and Energy (BMWI) under grant 20W1715B, as part of the LuFo-V project HYBSH-SAVE. The authors wish to thank Martin Blacha, Christian Reichensperger and Stefan Boehnel from Airbus Helicopters for great collaboration in this research project.

Authors contributions

Paul Schatrow: Conceptualisation, Methodology, Formal analysis, Investigation, Data curation, Writing - original draft, Writing - review & editing. Matthias Waimer: Conceptualisation, Methodology, Investigation, Data curation, Writing - review & editing. Marius Lützenburger: Conceptualisation, Methodology, Writing - review & editing.

Disclosure statement

The authors declare that they have no known competing financial interests or personal relationships that could have appeared to influence the work reported in this paper.

Funding

This article was supported by Bundesministerium für Wirtschaft und Klimaschutz (20W1715B).

ORCID

Paul Schatrow (b) http://orcid.org/0000-0002-1341-5884

References

- Baur S, Schickram S, Homulenko A, et al. Urban air mobility the rise of a new mode of transportation. Munich, Germany: Roland Berger GmbH; 2018.
- Holden J, Goel N. Fast-forwarding to a future of on-demand urban air transportation. San Francisco, USA: Uber Elevate; 2016.

- Grandl G, Ostgathe M, Cachay J, et al. The future of vertical mobility. Stuttgart, Germany: Porsche Consulting; 2018.
- Boelens J-H. Pioneering the urban air taxi revolution. Bruchsal, Germany: Volocopter GmbH; 2019.
- Shahab H. Urban air mobility (UAM) market study. Washington, DC: Crown Consulting Inc.; 2019.
- Rohit G, Reiche C, Fernando C, et al. Urban air mobility (UAM) market study. Washington, DC: Booz-Allen and Hamilton Inc.; 2018.
- eVTOL Aircraft Directory. Electric VTOL news by the vertical flight society. Available from: https://evtol.news/aircraft. (accessed October 2020 and May 2023).
- EASA. Special condition for small-category VTOL aircraft. EASA SC-VTOL-01 [2 July 2019; Issue 1]. Available from: https://www.easa.europa.eu/sites/default/files/dfu/SC-VTOL-01.
- EASA. Means of compliance with the special condition VTOL. [9] MOC SC-VTOL [12 May 2021; Issue 2]. Available from: https://www.easa.europa.eu/en/downloads/127717/en.
- [10] EASA. Second publication of means of compliance with the special condition VTOL. MOC2 SCVTOL [22 December 2022; Issue 3]. Available from: https://www.easa.europa.eu/en/downloads/137443/en.
- [11] EASA. Third publication of proposed means of complinace with the special condition VTOL. MOC3 SCVTOL [29 June 2022; issue 1]. Available: https://www.easa.europa.eu/en/downloads/138077/en.
- Stegeman B. eVTOL crashworthiness-moving forward. Presented at the NASA/FAA eVTOL Crashworthiness Workshop Series, Virtual Meeting #2, 2020 October 9. Available from: https://nari.arc.nasa.gov/events/crashworthiness/
- Federal Aviation Administration, Airworthiness criteria: special class airworthiness criteria for the Joby Aero, Inc. Model JAS4-1 powered-lift. Docket No. FAA-2021-0638; 2022. Available from: https://www.govinfo.gov/content/pkg/FR-2022-11-08/pdf/ 2022-23962.pdf
- Federal Aviation Administration. Airworthiness criteria: special class airworthiness criteria for the Archer Aviation Inc. Model M001 powered-lift. Docket No. FAA-2022-1548; 2022. Available from: https://www.govinfo.gov/content/pkg/FR-2022-12-20/pdf/2022-27445.pdf
- Dühne A. VTOL Crashworthiness based on EASA special condition. Presented at the NASA/FAA eVTOL Crashworthiness Workshop Series, Virtual Meeting #2, 2020 October 9. Available from: https://nari.arc.nasa.gov/events/crashworthiness/
- EASA. Certification specifications for normal-category aero-[16] planes. CS-23 Amendment 5; 2020. https://www.easa.europa.eu/ en/downloads/116297/en
- Littell J. Challenges for vehicle and occupant safety in autonomous electric vertical take-off and landing (eVTOL) vehicle crashworthiness. Presented at the 8th Biennial Autonomous VTOL Technical Meeting & 6th Annual electric VTOL Symposium; 2019 January 29-31; Mesa, AZ.
- Olivares G. Integrated safety concept. Presented at the Urban Transport Crashworthiness Workshop, Aerospace Structural Impact Dynamics International Conference; 2019 June 4-6; Madrid, Spain.
- [19] Foster L. Occupant safety opportunities with new generation aircraft. Presented at the NASA/FAA eVTOL Crashworthiness Workshop Series; Virtual Meeting #2; 2020 October 9.
- [20] Laarmann L, Welfens L, Röth T, et al. Crashworthiness review for electric vertical take-off and landing vehicles and implementation of the automotive safety approach. Presented at the APAC21-21st Asia Pacific Automotive Engineering Conference; 2022 October 3-5; Melbourne.
- [21] Laarmann L, Thoma A, Misch P, et al. Automotive safety approach for future eVTOL vehicles. CEAS Aeronaut J. 2023; 14(2):369-379. doi: 10.1007/s13272-023-00655-0.
- [22] Olivares G. Urban air transport crashworthiness - integrated safety approach. Presented at the Ninth Triennial International

- - Fire & Cabin Safety Conference; 2019 October 28-31; Atlantic City, NJ.
- [23] Littell J, Putnam J, Hardy R. The evaluation of composite energy absorbers for use in UAM eVTOL vehicle impact attenuation. Presented at the VFS 75th Annual Forum and Technology Display; 2019 May 13-16; Philadelphia, PA.
- [24] Olivares G. Integrated safety for eVTOL crashworthiness: from conceptual design to certification. Presented at the NASA/FAA eVTOL Crashworthiness Workshop Series, Virtual Meeting #3; 2021 April 13. Available from: https://nari.arc.nasa.gov/events/ crashworthiness/
- Putnam J, Littell J. Evaluation of impact energy attenuators and composite material designs of a UAM VTOL concept vehicle. Presented at the VFS 75th Annual Forum and Technology Display; 2019 May 13-16; Philadelphia, PA.
- Putnam J, Littell J. Crashworthiness of a lift plus cruise eVTOL vehicle design within dynamic loading environments. Presented at the Vertical Flight Society's 76th Annual Forum & Technology Display; 2020 May 19-21; Montreal, Quebec,
- Uber. eVTOL vehicle requirements and missions. 2018. https:// s3.amazonaws.com/uber-static/elevate/ Summary+Mission+and+Requirements.pdf
- Antcliff KR, Moore MD, Goordich KH. Silicon valley as an [28] early adopter for on-demand civil VTOL operations. Presented at the 2016 AIAA Aviation Forum; 2016 June 13-17; Washington, DC. Available from: https://ntrs.nasa.gov/api/citations/20160010150/downloads/20160010150.pdf
- Patterson MD, Antcliff KR, Kohlman LW. A proposed approach to studying urban air mobility missions including an initial exploration of mission requirements. Presented at the AHS International 74th Annual Forum & Technology Display; 2018 May 14-17; Phoenix, AZ.
- Zimmermann RE, Warrick JC, Lane AD, et al. Aircraft crash survival design guide volume III-aircraft structural crash resistance. USAAVSCOM TR 89-D-22C, 1989. https://apps.dtic. mil/sti/tr/pdf/ADA218436.pdf
- [31] Hurley TR, Vandenburg JM. Small airplane crashworthiness design guide. AGATEWP34-034043036; 2002. https://agate.niar. wichita.edu/Crashworthiness/WP3.4-034043-036.pdf
- [32] Bolukbasi A, Crocco J, Clarke C, et al. Full spectrum crashworthiness criteria for rotorcraft. RDECOM TR 12D12; 2011. https://apps.dtic.mil/sti/tr/pdf/ADA556604.pdf

- Waimer M. Development of a kinematics model for the assess-[33] ment of global crash scenarios of a composite transport aircraft fuselage. DLR-FB 2013-28; 2013. https://elib.dlr.de/88358/
- [34] Waimer M, Feser T, Schatrow P, et al. Crash concepts for CFRP transport aircraft - comparison of the traditional bend frame concept versus the developments in a tension absorbers concept. Int J Crashworthiness. 2017;23(2):193-218. doi: 10. 1080/13588265.2017.1341279.
- [35] Thyagarajan R, Ramalingam J, Kulkarni KB. Comparing the use of dynamic response index (DRI) and lumbar load as relevant spinal injury metrics. Presented at the ARL Workshop on Numerical Analysis of Human and Surrogate Response to Accelerative Loading; 2014 January 9. Available from: https:// apps.dtic.mil/sti/pdfs/ADA591409.pdf
- Stech EL, Payne PR. Dynamic models of the human body. [36] 1969. AMRL-TR-66-157; https://apps.dtic.mil/sti/tr/pdf/ AD0701383.pdf
- [37] Olivares G, Unger M. Accelerate eVTOLs crashworthiness design with an integrated safety development approach. Siemens Webinar. Available from: https://webinars.sw.siemens.com/de-DE/ evtols-crashworthiness-design/ (accessed 12 December 2020).
- [38] Vadlamudi S, Blundell M, Zhang Y. A multi-body systems approach to simulate helicopter occupant protection systems. Int J Crashworthiness. 2011;16(2):207-218. doi: 10.1080/ 13588265.2011.554203.
- [39] Busch M. Oleos. 2015. Available from: https://resources.savvyaviation.com/wp-content/uploads/articles_eaa/EAA_2015-04_ oleos.pdf
- Kindervater CM, Thomson R, Johnson AF, et al. Validation of crashworthiness simulation and design methods by testing of a scaled composite helicopter frame section. Presented at the American Helicopter Society 67th Annual Forum; 2011 May 3-5; Virginia Beach, VA.
- [41] Moore M, Warmoth A, Villa I. Elevate UAM mission, eVTOL requirements and common reference models. Presented at the Uber Elevate; 2018 May 8-9; Los Angeles, CA.
- United Nations. Recommendations on the transport of dangerous goods. ST/SG/AC.10/11/Rev.6; 2015. https://unece.org/ DAM/trans/danger/publi/manual/Rev.6/ST-SG-AC10-11-Rev6e_ WEB.pdf
- [43] EASA. Proposed means of compliance with the special condition VTOL. MOC SC-VTOL [25 May 2020; issue 1]. Available from: https://www.easa.europa.eu/en/downloads/114733/en